THE JOURNAL OF PHYSICAL CHEMISTRY C

pubs.acs.org/JPCC Article

Mechanistic Framework for the Formation of Different Sulfur Species by Electron Irradiation of *n*-Dodecanethiol Self-Assembled Monolayers on Au(111) and Au(100)

Natalia D. Aagaard, Julio C. Azcárate,* Jimena Olmos-Asar, Marcelo M. Mariscal, José Solla-Gullón, Eugenia Zelaya, and Mariano H. Fonticelli*

Cite This: https://dx.doi.org/10.1021/acs.jpcc.0c07106 Read Online

ABSTRACT: The electron-induced damage in self-assembled monolayers (SAMs) of *n*-dodecanethiolate on Au(111) and Au(100) single-crystalline surfaces is investigated in situ by X-ray photoelectron spectroscopy. The same irradiation dose produced different adsorbed groups. The damage at the headgroup−substrate interface leads to find dialkyl sulfide (RS−R′) on Au(111), while dialkyl disulfide (RS−SR) and/or thiol (RSH) were produced on Au(100). With regard to C species, significant amounts of C═C are generated on Au(111) but not on Au(100), showing that double bond formation is not triggered through the same pathways on these surfaces. Detailed analysis of a variety of mechanisms, which involved cationic (RS^+), anionic (RS^-), or thiyl radical ($RS^\bullet$) species, in combination with *ab initio* density functional theory (DFT) calculation, leads to the conclusion that the radical pathways successfully explain the experimental results. Molecular dynamics simulations show that the *n*-dodecanethiolate SAMs on both surfaces are equivalent with regard to the van der Waals interactions. The breakage of the S−Au bonds is studied by means of DFT calculations. The thiyl radical would form close to the Au(100) surface, making it likely to react with another thiyl radical or thiolate to form the RS−SR species. On the other hand, for Au(111), the thiyl radical would form farther from the surface, reacting with the alkyl chains of neighboring molecules to form RS−R′ species. The mechanistic framework proposed here is very useful to explain the behavior of related systems.

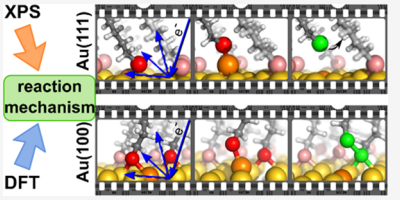

1. INTRODUCTION

Self-assembled monolayers (SAMs) are versatile systems to investigate the surface science phenomena and to make progress in nanotechnology.[1−3] Among many molecular adsorbates that form SAMs, thiols on metallic and semiconductor surfaces are considered model systems. Moreover, renewed interest in fundamental research on thiolate SAMs has been observed. For instance, the molecular origin of the odd−even effects[4] and whether a dipolar group modifies electron tunneling across SAMs[5] have been recently studied. The interest has been mainly triggered due to a wide range of applications of thiolate SAMs in molecular electronic devices.[6−8] The uses of SAMs for surface patterning, microcontact printing, and scanning probe lithography are examples of methods based on the transfer of molecular components.[3] However, the attainable resolution with these methodologies might be limited due to the diffusion of the thiols when delivered to the surface.[9,10] On the other hand, preformed SAMs can be accurately patterned by selective damaging with light (e.g., lasers, ultraviolet light, X-rays) or particle beams (electrons, ions).[11−16] Interestingly, the resolution of these lithographs is determined by the size of the beam applied to the SAM,[3] with the implementation cost and the need for precise control of the damaging[17] process being the main factors that represent potential disadvantages. For this reason, the study of radiation damage (by electrons or X-rays) in SAMs is important to improve lithographic processes.

The exposure of SAMs to ionizing radiation or low-energy electrons results in a series of complex and interrelated processes. These processes include the loss of orientational and conformational order, partial dehydrogenation, formation of a cross-linking network between the SAM constituents, desorption of film fragments and individual molecules, and damage of the headgroup−substrate interface.[18−20] With regard to sulfur-containing species produced upon irradiation of SAMs on Au(111), dialkyl sulfides (RS−R′) are proposed as the main products, but small amounts of atomic sulfur are formed in a process that strongly depends on temperature.[21] Not only the primary beam-induced damage,[17,22] also the secondary electrons[23,24] are involved in the chemical transformations of SAMs. Following this idea, the damage is expected to occur when the radiation used to analyze the specimen generates low-energy electrons, either when the

Received: August 3, 2020
Revised: September 8, 2020
Published: September 17, 2020

beam is composed of electrons or photons. Therefore, the photon-irradiation damage can be closely related to that observed when electrons are used as probes. In some cases, the irradiation damage has been rationalized in the context of Desorption Induced by Electronic Transition (DIET),[25] Electron Stimulated Desorption (ESD),[26] or Dissociative Electron Attachment (DEA).[26] The few proposed reaction mechanisms were mainly centered on the organic backbone degradation.[18,26−29] Apart from a few examples, like the disulfide formation from neighboring thiyl radicals,[30] scarce contributions for the understanding of reaction mechanisms were proposed to interpret the irradiation-derived species.

Although RS−R′ species form when dodecanothiol SAMs on Au(111)—or (111) textured thin films—are irradiated,[31] the chemical nature of the products is not discussed in such deepness for other substrates. While the same X-ray photoelectron spectroscopy (XPS) signal assignment can be done for damage-related species for dodecanethiolate (DDT) on Ag[32,33] and Cu,[33] the binding energy (BE) of the S $2p_{3/2}$ signal associated with damaged species is compatible with thiol (RSH) or disulfide species (RS−SR) for DDT on a Pt(111) single-crystalline surface.[34] Therefore, the nature of the substrate can play a relevant role in the determination of the degraded products. In this regard, the present paper shows a comparison of radiation damage for DDT SAMs on Au(111) and Au(100) single-crystalline surfaces. SAMs on Au(100) have been scarcely studied in comparison with those grown on Au(111) preferred-oriented or single-crystalline substrates. According to the electrochemical[35,36] and thermal[37] desorption studies and density functional theory (DFT) calculations and simulations,[1,38−41] thiolate SAMs on Au(100) seems to be thermodynamically more stable than on Au(111). However, it is not straightforward to hypothesize that SAMs on Au(100) are more resistant than on Au(111) against irradiation damage. On the contrary, the oriented-attachment of thiol-protected gold nanoparticles through Au(100) faces during the transmission electron microscopy (TEM) session can be interpreted as a consequence of preferential desorption from the more open and reactive surfaces like (100) instead of (111).[42] Therefore, it is essential to make a valid comparison on how the alkanethiolate SAMs degrade when they are on Au(100) or Au(111) surfaces.

We found that while sulfides were formed on the Au(111) crystal modified by dodecanethiol, disulfides were the main species on Au(100). To the best of our knowledge, there are no antecedents on radiation-induced degradation of alkanethiolatate SAMs on Au(100). We performed our study by means of electron irradiation and XPS since (a) electron-related damage is present whatever was the nature of the primary beam and (b) we are interested in the chemical nature of the products that remain adsorbed along the irradiation process. The experimental evidence is further supported by means of density functional theory (DFT) calculations and classical molecular dynamics (MD) simulations. Notably, this is the first damage study of the DDT SAMs on Au(100) and also the first study on the reaction mechanism to understand why each sulfur species is formed. Finally, we propose a rational explanation for thiol SAM degradation induced by electron irradiation. This new mechanistic framework will provide support to interpret the behavior of SAMs of other adsorbates and different substrates under a wide variety of experimental conditions.

2. EXPERIMENTAL AND CALCULATION DETAILS

Two types of Au substrates were used. The Au(111) single crystal was a disk of 9 mm diameter and 2.5 mm thickness purchased in Princeton Scientific Corp. Its surface was cleaned by sputtering with Ar ions and was annealed at 450 °C in a UHV chamber. The Au(100) single crystal was a Clavilier-type bead crystal, oriented, cut, and polished as reported previously.[43] Its surface was cleaned with Piranha solution and rinsed with Milli-Q water, followed by flame annealing.[44] SAMs on both single crystals were prepared by immersion overnight in 25 μM solution of dodecanethiol (≥98% Aldrich) in absolute ethanol (anhydrous for HPLC-Plus-Gradient Carlo Erba). After the self-assembly, the crystals were thoroughly rinsed with absolute ethanol to eliminate the excess of thiol, blow-dried with nitrogen, and quickly entered into the vacuum chamber for experiments.

The irradiation procedure was performed with a SPECS EQ. 22/37 electron gun. It was set to generate 600 eV electrons and a current density (j) of 1 μA cm^{-2} ($i \sim 0.25$ μA in an irradiated area of 0.24 cm^2) during constant time pulses. The accumulated irradiation doses were calculated by a multiplication between the current density and the irradiation time.

To analyze the effect of electron radiation, XPS measurements were performed with a SPECS Phoibos 150 analyzer using a monochromatized Al Kα (1486.6 eV) X-ray source. The characterization was performed at room temperature at a base pressure lower than 5×10^{-10} mbar. XP spectra were obtained for pristine SAMs and after each electron irradiation step. Special care was taken to minimize the X-ray-induced damage. XP spectra were acquired at 20 eV energy pass, 0.05 eV energy step, and a 0.1 s dwell time. The acquisition order was S 2p, Au 4f, C 1s, and valence band (VB) regions. Double check for the energy scale was performed by fitting the Fermi Edge in the VB region and Au 4f spectra. The Au 4f spectra were fitted with a doublet of Doniach-Sunjic functions and a Shirley-type background, fixing the Lorentzian width to 0.317 eV and the asymmetry parameter to 0.052.[45] Each component of the S 2p region was described by one S $2p_{3/2}$ and S $2p_{1/2}$ doublet. These components were fitted with a doublet of symmetric Voigt functions with the same Gaussian width, fixing the Lorentzian width at 0.2 eV. The spin−orbital splitting of both peaks was fixed to 1.18 eV and the area ratio between both peaks was fixed at 0.5 (S $2p_{1/2}$/S $2p_{3/2}$). The spectra were fitted using two components. The component characteristic of the thiolate (S2) was fixed with the binding energy and the gaussian width such as that obtained in the pristine SAM fit. Then, a second component (S3) was added to take into account the irradiation-induced sulfur species. The binding energy and gaussian width of this component were fixed such as that obtained in the fit of the last acquired spectrum. The C 1s spectra were fitted by a single symmetric Voigt function fixing the Lorentzian width at 0.2 eV. The whole data set was fitted self-consistently.

Ab initio calculations were performed within the density functional theory (DFT) approach[46] using the Quantum-Espresso Package[47,48] with ultrasoft pseudopotentials.[49] The exchange and correlation terms were described through the generalized gradient approximation (GGA) in the Perdew−Burke−Ernzerhof (PBE)[50] implementation. The gold surfaces were simulated with a 3×3 supercell composed of 4 Au layers at its DFT predicted equilibrium lattice parameter. A vacuum of 15 Å in the perpendicular direction to the surface plane was

https://dx.doi.org/10.1021/acs.jpcc.0c07106
J. Phys. Chem. C XXXX, XXX, XXX−XXX

used to avoid spurious interaction between periodic images. The first Brillouin zone was sampled with a 6 × 6 × 1 grid centered at the Γ point. Geometry optimizations were done freezing the bottom-most Au layer in its bulk position and relaxing the remaining atoms until the individual forces and the energy difference between consecutive optimization steps were smaller than 0.01 eV $Å^{-1}$ and 0.001 eV, respectively. Van der Waals (vdW) interactions were implemented with the Grimme-D3 method.[51]

To obtain vdW interactions of compact monolayers on gold, classical canonical molecular dynamics (MD) simulations were done. A bond-order Morse-like potential[41] was used to represent the atomic interaction of the complex S−Au interface, whereas the second-order approximation of the thigh binding (SMTB) theory was employed to model the Au−Au interactions,[52] and the Universal Force Field (UFF) was used to represent the inter- and intramolecular interactions of the alkanethiol molecules using the same potential parameters as reported in ref 41. These interactions include bond stretching, bond bending, and torsional and dispersion forces. For the last ones, a cut-off of 1 nm was used. For the MD simulations, a home-made code was used, where the Ermak algorithm was implemented to obtain the trajectories following the Langevin equations of motion. The temperature was kept at 300 K. The dynamic is allowed to proceed until we reach a stationary stage. At this point, the vdW contribution to the total energy (due to intermolecular interactions) was extracted and divided by the number of adsorbed molecules.

3. RESULTS AND DISCUSSION

The irradiation-induced damage of SAMs on metals[53,54] and semiconductors[55] has been studied extensively. Scanning tunneling microscopy (STM), scanning electron microscopy (SEM), and infrared reflection-absorption spectroscopy (IRAS) are useful to monitor the structural changes, whereas chemical degradation has been probed mainly via XPS,[17,23,31,53,54] near-edge X-ray absorption fine structure (NEXAFS),[23,32,53] temperature-programmed desorption (TPD),[56] mass spectrometry (MS),[57] and infrared spectroscopy (IR).[58] Very often, the measurements are not sufficient to discern which processes are involved in SAMs' degradation since they are sensitive to the species that remain in the film or, alternatively, to the desorbed side products. XPS is a valuable and versatile tool to investigate the chemical nature of the adsorbed species. In particular, recent studies on the radiation-induced damage of thiolate SAMs were based on XPS measurements.[16,17,56]

The SAMs are carefully characterized taking special care to minimize the radiation damage caused by the XPS measurement itself. The damage observed during an XPS experiment is mainly due to the secondary electrons (slow electrons, <50 eV) generated by the inelastic scattering of the fast core-level photoelectrons and Auger electrons during their travel through the inner to the sample surface (see the Supporting Information) and not by the incident X-rays themselves.[54,59] Therefore, the measurements were carried out to get good signal/noise ratios and an acceptable level of damage. The dose of secondary electrons due to the X-rays after each cycle of XPS measurements—S 2p, C 1s, and Au 4f regions—is equivalent to only 0.02 s of irradiation with electrons (for details, see the Supporting Information). In other words, the damage during XPS measurement can be neglected. The XPS data show full alkanethiolate layers grown on both single crystals. This is in good agreement with previous reports.[23,35,37]

The overall changes in Au 4f, C 1s, and S 2p using electron irradiation were widely reported in the literature.[23,32,53,54] The Au 4f signal increases, while the C 1s decreases due to the loss of material as the irradiation progresses (see representative spectra in the Supporting Information). The changes in S 2p are a bit more complex because, although it also decreases due to material loss, the DDT moieties in the pristine SAM are transformed into other sulfur species. Indeed, some unrevealed aspects can be distinguished comparing the effects of radiation-induced damage in SAMs on different crystalline Au surfaces.

Figure 1 shows the S 2p XPS region of different single-crystalline Au surfaces covered by DDT. The spectra on panels

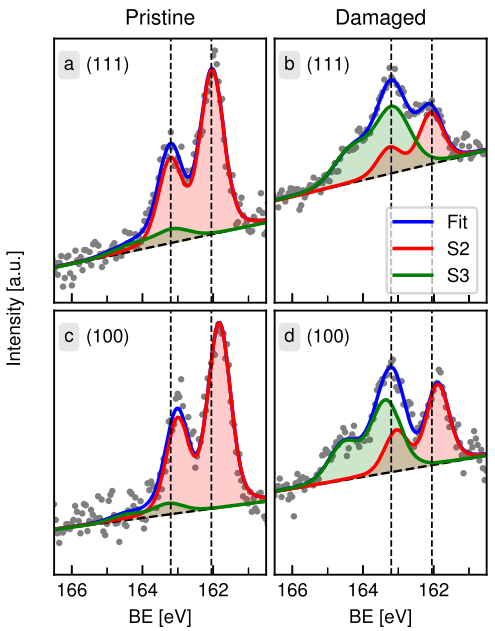

Figure 1. Panels (a) and (c) show the S 2p XP regions for pristine SAMs on Au(111) and Au(100), respectively, while the spectra on (b) and (d) show the S 2p region after exposure to 600 eV electrons. The electron doses on (b) and (d) are 0.84 and 0.88 mC cm^{-2}, respectively.

a and c correspond to pristine SAMs that are irradiated with a minimum dose of X-rays necessary to get good quality data. These spectra are fitted with one S 2p doublet at BE ∼162 eV (S2), and a minor contribution at higher BE ∼163−164 eV (S3).[60−62] The S2 component is related to chemisorbed thiolate on the metal surface through a covalent bond (RS-Au), while the S3 component is assigned to unbound thiol (RSH), RS−R′ and/or RS−SR species.[31,60] Note that no S1 component (BE ∼161 eV), which is usually associated with dilute atomically adsorbed sulfur,[19,21,62−65] has been found in our spectra.

In good agreement with previous reports, the S2 has a BE of 162.05 eV for DDT on Au(111),[63] while it is 161.85 eV for Au(100).[35,37,66] According to Arisnabarreta et.al., this BE shift is associated with larger electronic charge transfer from the Au to the S in the case of the (100) surface.[66] The irradiation with 600 eV electrons produced huge damage, which is revealed by a decrease of the S2 signal and a concomitant increment of S3 (Figure 1b,d). The results for the (111) surface are in complete agreement with previous reports.[24,63] Indeed, the

https://dx.doi.org/10.1021/acs.jpcc.0c07106
J. Phys. Chem. C XXXX, XXX, XXX−XXX

spectrum in Figure 1b is accurately fitted with one S2 component located at 162.05 eV, while the BE of the S3 component resulted in 163.1 eV. Among the many assignments for the sulfur species on damaged SAMs (see for instance the excellent reviews by Duwez[54] and Zharnikov[67]), the most reliable interpretation is provided by Heister et al.[31] The authors found that the BE of the damaged sulfur (S $2p_{3/2}$ at 163.14 eV)[31] for SAMs on preferentially oriented Au(111) is consistent with the predominance of RS−R′ moieties. On the other hand, the S3 BE is 163.4 eV for the DDT SAMs on Au(100) (Figure 1d). In addition, for extensively damaged SAMs, the full width at half-maximum (FWHM) of S3 for DDT SAMs on Au(111) is higher than that on Au(100), 1.16 and 0.99 eV, respectively. However, the S2 component has a very similar FWHM for both surfaces: 0.75 eV for (111) and 0.74 eV for (100). Previous studies on pristine alkanethiolate SAMs on Au(100) and Au(111) have omitted the difference in the BE of S3 since its relative contribution was very low.[35] Indeed, high uncertainty in the BE and FWHM values would be expected for any low-intensity peak. On the contrary, the extensively damaged SAMs have great contributions of S3, which allowed reliable fits. The remarkable difference in S3 BEs is attributed to initial state effects (chemical shifts) since damaged species can remain throughout the entire film.[31] In addition, the S_n aggregates—S $2p_{3/2}$ at about 163 to 164 eV[68,69]—are dismissed since damaged SAMs have not shown sulfur excess. The C/S atomic ratios are above 12 for all of the SAMs along their irradiation. Moreover, the absence of S1 is in agreement with no elemental sulfur formation. Then, we associated the S3 on Au(100) to RS−SR and/or thiol (RSH) damage products but not to RS−R′ as proposed for Au(111).[31]

The intensity of the C 1s signal steadily decreases with the increment of the damaging processes (see the Supporting Information). This is attributed both to the loss of material due to the degradation of SAMs and also to the desorption of adventitious carbon. As the contributions from the adventitious carbon are low—smaller than 10%, and their behavior might be the same for both Au faces, the difference in C 1s shape evolution should be due to intrinsic changes in the SAMs. Figure 2, panels a and b, shows how the shape of the normalized C 1s signals changes with the increment of irradiation dose. The evolution of C 1s for DDT on Au(111) follows the already reported behavior.[31,32,53] The monotonical shift to lower BEs (Figure 2a, see the Supporting Information for the whole series of peaks) and an increment in the normalized intensity between 284 and 284.5 eV are associated with C═C bonds, which are produced due to radiation-induced H loss.[23,31,32,53] Additionally, a vibrational contribution at higher BEs[70−72] can be noticed. The broadening and the shift to lower BE of C 1s were also observed for alkaneselenolates on Au(111).[73] On the other hand, the most important change in the C 1s signal for DDT on Au(100) is the increment of vibrational contributions at higher BEs due to electron irradiation. It is expected that the H loss and the consequent formation of C═C by direct interaction of the electrons with the alkyl chains should be equivalent for both SAMs. However, it is clear that a larger amount of C═C is present in irradiated DDT SAMs on Au(111) than on Au(100). Then, the C═C increment in Au(111) cannot be solely associated with H loss by a simple interaction between alkyl chains and electrons. Notably, the C 1s evolution on Au(100) resembles the behavior of the monolayers derived

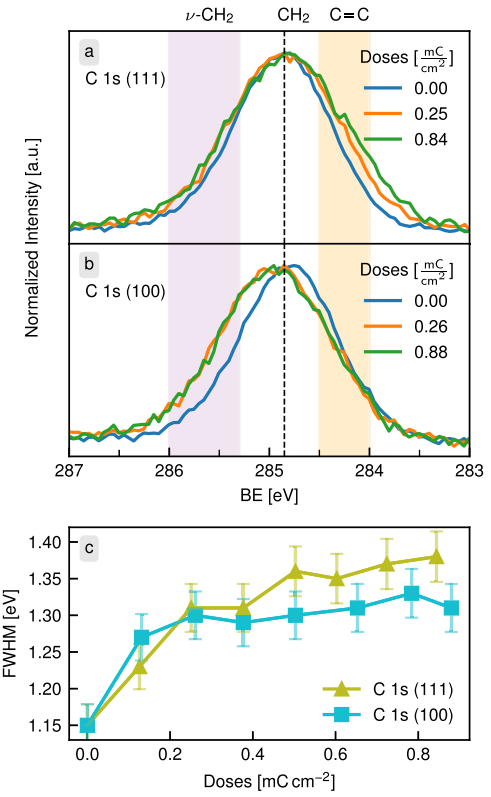

Figure 2. (a) and (b) show normalized C 1s spectra of DDT SAMs on Au(111) and Au(100), respectively, for different electron irradiation doses. (c) C 1s FWHM vs Doses from the complete data set.

from cyclic alkanethiols on Au(111)[58] and other adsorbates—silanes[29] or carboxylic acids[74]—on various substrates, i.e., an increment in the FWHM (Figure 2c) and a shift to higher BEs due to their irradiation. Another important footprint of the changes in the conformation of alkyl chains and the formation of new carbon species is the increment of the FWHM.[17,75] The C 1s peaks are slightly wider for irradiated SAMs on (111) than on the (100) surface, as can be seen from the FWHM vs dose representation (Figure 2c). Therefore, it is reasonable to propose that the predominant formation of C═C groups, typical of alkanethiolates on Au(111), is not expected for all kinds of SAMs. However, the loss of alkyl-chain organization could be considered a more general process, which is evident for the DDT degradation on Au(100). Consequently, it is necessary to provide a mechanistic approach that considers the differences between SAMs.

Considering that different sulfur and carbon species are formed on each surface, we analyze different reaction mechanisms. Moreover, we support our reasoning with molecular dynamics simulations and DFT calculations. These mechanisms must explain the predominant formation of RS−R′ and C═C species for irradiated DDT SAMs on Au(111), and also the generation of RS−SR and/or RSH products on Au(100) without a great amount of C═C groups.

The first step that the mechanism should involve is the interaction of a slow electron with an absorbed thiolate. According to DIET and ESD concepts, this adsorbate−electron interaction could result in electron impact ionization (forming a cationic entity, RS^+), electron attachment (forming an anionic entity, RS^-), or electron impact excitation (which can form a thiyl radical, $RS^\bullet$).[59] These new entities act as

https://dx.doi.org/10.1021/acs.jpcc.0c07106
J. Phys. Chem. C XXXX, XXX, XXX−XXX

reactants to initiate different chemical reactions. The energy of the charged species can be formally related to that of the thiyl radical by considering the following processes

$$RS - Au \rightarrow RS^{\bullet} + Au_{(surf)} \quad (1)$$

$$RS^{\bullet} + e^{-} \rightarrow RS^{-} \quad (2)$$

$$RS^{\bullet} \rightarrow RS^{+} + e^{-} \quad (3)$$

The first reaction corresponds to the formation of a thiyl radical and an Au site. The second and third reactions involve, respectively, the gain or loss of an electron by the thiyl radical. We calculated the energy required to form the anion RS^{-} ($E_{RS^{-}}$) from $RS^{\bullet}$ and an electron on Au (eqs 1 and 2)

$$E_{RS^{-}} = WF + EA \quad (4)$$

where WF is the work function of the Au(*hkl*) surface and EA is the electronic affinity of the radical in a vacuum, calculated as $E_{RS^{-}} - E_{RS}$ (−2.71 eV). Finally, the cation formation, draining the electron in the Au surface, results in energy change of (eqs 1 and 3)

$$E_{RS^{+}} = IE - WF \quad (5)$$

where IE = $E_{RS^{+}} - E_{RS}$ (8.41 eV) is the ionization energy of the radical in a vacuum.

Thus, we were able to calculate the formation energy of the two charged species near both single-crystal surfaces, taking into account that the WF of clean surfaces differs from functionalized ones (see for example ref 76 and references therein). As can be seen in Table 1, in all cases, the creation of the ions is an endergonic process.

Table 1. Energies (in eV) Involved in the Creation of Ions near the Gold Surfaces for Both Low- and High-Coverage Cases

	low coverage			high coverage		
surface	WF	$E_{RS^{-}}$	$E_{RS^{+}}$	WF	$E_{RS^{-}}$	$E_{RS^{+}}$
Au(111)	5.23	2.52	3.18	3.74	1.03	4.67
Au(100)	5.08	2.37	3.33	3.64	0.93	4.77

The above results clearly show that both charged species, RS^{-} and RS^{+}, are more energetic than the thiyl radical. Then, the most probable reactant to be formed is $RS^{\bullet}$. To further support the plausibility of this radical as an intermediate, we have calculated the magnetization of a system consisting of a Au(111) surface and an $RS^{\bullet}$ desorbed from it. We found that the most stable state is the one with a total magnetization of 1 (i.e., one unpaired spin). The density of states projected on the sulfur orbitals shows an unoccupied p orbital, with spin down. Finally, the spatial localization of the spin was found to be on the sulfur atom. These results are shown in Figure S5 and support the mechanism through a thiyl radical $RS^{\bullet}$.

Anyway, to elucidate an adequate reaction mechanism, we need to evaluate all reasonable alternatives, even taking into account the energetically less favorable species. We must also consider that the desorption of alkyl chains is restricted by mass transport limitations due to their efficient packing within the SAMs.[77] The pathways initiated by RS^{-} and RS^{+} are discarded because they cannot even qualitatively explain the XPS results. Those mechanisms are described in detail in the Supporting Information.

In Scheme 1, we represent a reaction mechanism that successfully explains our experimental results. (1) After the

Scheme 1. Reaction Mechanisms Initiated by Thiyl Radical, $RS^{\bullet}$

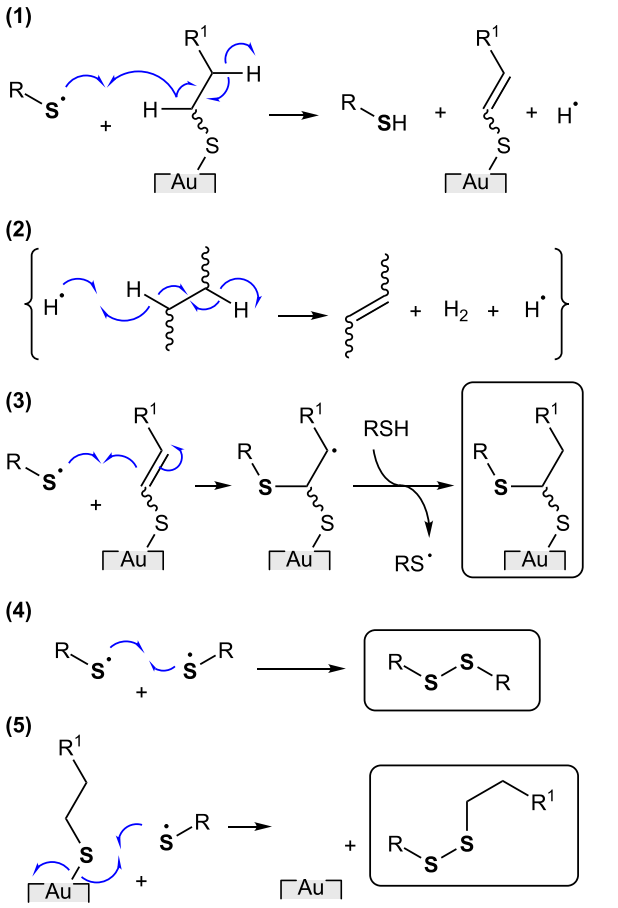

thiyl radical is formed by the secondary electrons, this radical can react with a neighboring alkyl chain, leading to a C═C and a $H^{\bullet}$. (2) Indeed, the formation of C═C is a common feature in the free radical chain mechanism involving rapid $H^{\bullet}$ transfer through the surface overcoming the classical diffusion limitations as like as in the bulk solution.[18,77,78] (3) Next, the thiol−ene reaction to form RS−R′ moieties is also promoted.[79] The termination reactions involve (4) the union of two thiyl radicals or (5) one thiyl radical with a neighboring thiolate, which in this case form RS−SR and do not form C═C. Therefore, the radical route appears to be a better mechanism to explain the formation of different chemical species (RS−R′, RSH, RS−SR, and C═C), which are formed on both surfaces. However, this mechanism cannot explain by itself why different products are preferably formed on each studied surface. Then, it is proper to consider how molecular packing can influence the reaction mechanism.

In the following, we analyze whether vdW interactions and/or the differences among the molecular arrangements of the adsorbates on the Au(111) and Au(100) influence the observed preferred products on each facet. We performed a classical molecular dynamics simulations with a semiempirical force field.[41] In the case of the (111) face, the $\sqrt{3} \times \sqrt{3}\ R30°$ structure was simulated, and for the (100) face, we studied the $c(2 \times 2)$ lattice. After molecular relaxation, the tilt angle with

https://dx.doi.org/10.1021/acs.jpcc.0c07106
J. Phys. Chem. C XXXX, XXX, XXX−XXX

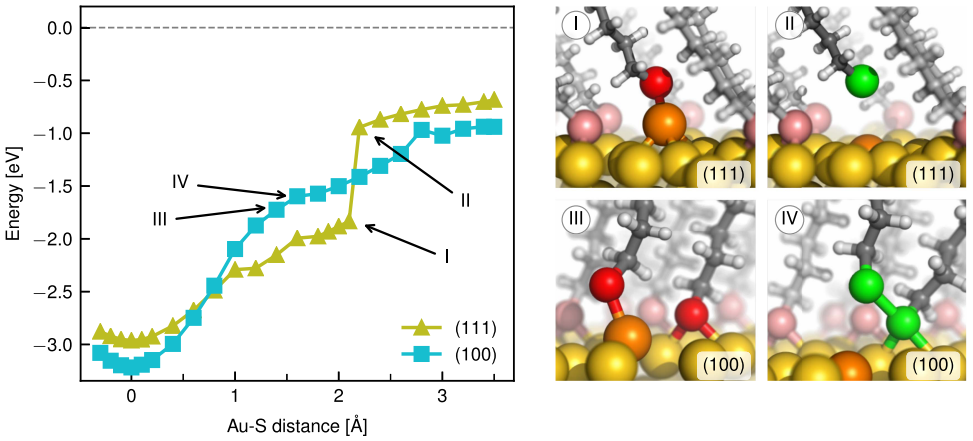

Figure 3. Left panel: Energy vs vertical distance between the S atom and the gold surface for both (111) and (100) facets at high coverage. The origin of the abscissa corresponds to the equilibrium Au−S distance. Right panel: snapshots of the local atomic configuration before and after the break of Au−S bonds for the pulled molecules on each Au surface. (I) and (III) correspond to the Au−S distance just before the bond break for the (111) and (100) surfaces, respectively. The gold adatom pulled is highlighted in orange. In (II) the detachment of an RS$^{\bullet}$ is highlighted by the sulfur atom in green, while in (IV) the S−S bridge is remarked.

respect to the surface normal resulted to be ∼33° for DDT-Au(111) and ∼10° for DDT-Au(100), which are in good agreement with the reported experimental results (30 and 14°, respectively).[80] Since the forces in this classical approximation are additive, it is possible to isolate the energy corresponding to vdW intermolecular interactions. We averaged five runs of 1 ns for each surface and finally divided the total vdW energy by the number of adsorbed DDT molecules. For both cases, we found that the contribution to the energy coming from noncovalent dispersion forces is −0.81 eV/molecule. The result that the vdW energy is equal for (111) and (100) facets is supported by the fact that the molecular density on both surfaces is very similar.[81] This indicates that, considering the vdW intermolecular forces, we should not expect differences in desorption behavior when the (111) and (100) surfaces are fully covered. However, the vdW forces restrict the displacement of the thiyl radical within the SAM. Thus, these interactions promote or hinder some of the reactions described above (Scheme 1) and even the readsorption process.

Since the molecules in confined spaces can react differently than those in bulk,[77,78,82,83] it is necessary to consider how structural differences in the SAMs can modify the reaction mechanism. Therefore, we considered the desorption of thiol adsorbates through the analysis of Energy vs distance plots for pentanethiol moieties obtained by means of *ab initio* calculations. We compare the molecular desorption of pentanethiolate, as radical from Au(111) and Au(100) at the high-coverage condition. The energy is recorded as we pull out a molecule from the surface, by increasing a distance of 0.2 Å in each step while keeping the height of its S atom fixed and relaxing the rest of the system. The energy profiles with some representative snapshots are shown in Figure 3.

A close inspection of the atomic configuration during desorption shows that in both surfaces a gold adatom is pulled attached to the RS at the initial stages of the process (Figure 3I,III, orange highlighted). However, we observe two main differences. On one hand, for the case of Au(111), there exists evident energetic stabilization when the adatom is displaced together with RS, which appears as a jump in the energy profile when it comes back to the surface. The Au−S bonds break when S is at 2.1−2.2 Å from the surface. In this configuration, the distance between the RS and the nearest S atom is 4.3 Å, while it is 2.7 Å to the nearest H−C neighbor (Figure 3II). On the other hand, for the Au(100) case, there is no clear stabilization associated with this process. However, it can be noted that when the S is pulled 1.6 Å (i.e., going form III to IV in Figure 3) the Au adatom returns to the surface. In this configuration, the distance between the RS and the nearest S is 2.3 Å, while it is 3.1 Å to the nearest H−C neighbor (Figure 3IV). It is very important to note that the typical S−S bond length is 2.05 Å. Then, the distance of 2.3 Å can be associated with a new S−S bond between the RS and a neighboring thiolate (green highlighted in Figure 3IV). These results support the mechanisms proposed for thiol desorption on both surfaces. In the case of Au(111), the thiyl radical would be formed far from the surface, and it is able to react with the alkyl chains of neighboring molecules, forming the RS−R′ species. On the other hand, on Au(100), the thiyl radical would be formed much closer to the gold surface and it could react with another thiyl radical or adsorbed thiolate to form the RS−SR species.

The proposed reaction mechanism constitutes a mechanistic framework, which can be useful to interpret the behavior of other systems. For example, it can also explain why irradiated SAMs of cyclic aliphatic thiols on preferentially oriented Au(111) present an S3 component at 163.4 eV, C 1s shifts to higher binding energies upon their irradiation, and C═C was not observed by the near-edge X-ray absorption fine structure (NEXAFS).[58] According to Waske et al., the organic moieties stay in place under electron irradiation and cross-link to one another, preventing irradiation-induced desorption.[58] Within our mechanistic framework, the closeness of the headgroup to the Au substrate is what determines the kinds of products found in that article. Moreover, the authors stated that the irradiation effects in the S−Au interface are smaller for these thiols than for linear alkanethiols. The same concepts are useful to explain the atomic sulfur formation when DDT SAMs were irradiated at low temperature (60 K).[19,25] The molecular mobility is drastically diminished and the readsorption process is highly favorable under these conditions. Therefore, the formation of atomic sulfur due to the irreversible C−S bond scission, which is in competition with the reversible Au−S bond break, becomes significant in cryogenic conditions. As final remarks, we would like to stress that alkanethiolate SAMs

https://dx.doi.org/10.1021/acs.jpcc.0c07106
J. Phys. Chem. C XXXX, XXX, XXX−XXX

on Ag and Cu lead to S3 contributions compatible with dialkyl sulfide moieties (S3 ~163.2 eV).[33] On the other hand, a radiation damage study of DDT on a Pt(111) single-crystal showed that BE for S3 resulted to be 163.54 eV,[34] which can be associated with thiol and/or disulfide formation. Nevertheless, the relevant difference in the S3 BE is overlooked until now. We believe that the phenomena responsible for the differences in the chemical behavior of the discussed systems have common elements. Thus, we expect that this paper will encourage further studies that would provide a deeper understanding of the detailed processes responsible for the electron-induced radiation damage of SAMs. Moreover, this novel viewpoint can be useful to choose the best options among the variety of surfaces and molecules for electron lithography engineering, according to the specific application.

5. CONCLUSIONS

We have studied the radiation-induced damage of dodecanethiolate SAMs on Au(111) and Au(100) single-crystalline surfaces by means of XPS. In addition to the loss of organic material, the irradiation with low-energy electrons leads to different S and C species. While RS−R′ was found for irradiated dodecanethiolate SAMs on Au(111), RS−SR was produced on Au(100). With regard to the C species, significant amounts of C═C were generated on Au(111), but the most evident process on Au(100) is the loss of alkyl-chain organization. We considered a variety of phenomena to explain the experimental results, which allows the buildup of a useful mechanistic framework. First, since molecular desorption might be governed by van der Waals interactions, we carried out molecular dynamics simulations, which have shown that the dodecanethiolate SAMs on both surfaces are equivalent in this regard. Second, three sulfur species were accounted as reaction initiators, thiyl radicals, and cationic and anionic species. However, only the radical-based mechanism explains the experimental data set. Moreover, our calculations show that the reaction pathways that involve the radical would have lower energies than those with charged species. The thiyl radical can react with a hydrocarbon chain to form a C═C moiety, which then reacts with another thiyl radical, leading to RS−R′. Within the same framework, two thiyl radicals or one radical and one adsorbed thiolate can form RS−SR species. Finally, since the reacting species are confined within the SAMs, we have studied in detail the energetics behind the S−Au rupture by means of DFT calculations. We found that the thiyl radical would be formed far from the Au(111) surface, and it is able to react with the alkyl chains of neighboring molecules, forming the RS−R′ species. On the other hand, on Au(100), the thiyl radical would be formed much closer to the gold surface and it could react with another thiyl radical or an adsorbed thiolate to form the RS−SR species.

As final remarks, we would like to stress that SAMs of thiols on Au(111) surfaces have been considered a model system for a long time. Although comparisons of many two-dimensional molecular layers with them have been very useful, our study represents an example of how this approach is usually overestimated. It has been shown that the surface chemistry of thiols on many metals is different than that found on Au(111), for instance, with regard to the tendency to produce atomic sulfur, which was confirmed for many metals[84−87] but for Au(111). Moreover, slight changes in the organic backbone can induce the breaking of the S−Au bond,[65] which highlights that also the chemical nature of the thiol matters. Altogether, the proposed mechanism provides a rational framework to understand the behavior of other thiol−metal interfaces along irradiation experiments and widens the perspective of SAMs' surface chemistry.

■ ASSOCIATED CONTENT

Supporting Information

The Supporting Information is available free of charge at https://pubs.acs.org/doi/10.1021/acs.jpcc.0c07106.

Description of the secondary-electron energy distribution; comparison of the damage from the electron beam and X-rays; XPS spectra evolution upon irradiation: C 1s, Au 4f, and S 2p signals, density of states projected on sulfur orbitals of the thiyl radical; reaction mechanisms initiated by RS^- and RS^+ (PDF)

■ AUTHOR INFORMATION

Corresponding Authors

Julio C. Azcárate − *Centro Atómico Bariloche (CAB), Comisión Nacional de Energía Atómica (CNEA)—CONICET, San Carlos de Bariloche, R8402AGP, Argentina;* orcid.org/0000-0002-1114-4611; Phone: +54 294 444 5147; Email: jcazcarate@cab.cnea.gov.ar; http://fisica.cab.cnea.gov.ar/metales

Mariano H. Fonticelli − *Instituto de Investigaciones Fisicoquímica Teóricas y Aplicadas (INIFTA), Departamento de Química, Facultad de Ciencias Exactas, Universidad Nacional de La Plata (UNLP)—CONICET, La Plata B1900, Buenos Aires, Argentina;* orcid.org/0000-0003-1739-9620; Phone: +54 221 425 7430; Email: mfonti@inifta.unlp.edu.ar; http://nano.quimica.unlp.edu.ar

Authors

Natalia D. Aagaard − *Centro Atómico Bariloche (CAB), Comisión Nacional de Energía Atómica (CNEA)—CONICET, San Carlos de Bariloche, R8402AGP, Argentina*

Jimena Olmos-Asar − *Instituto de Investigaciones en Fisicoquímica de Córdoba (INFIQC) CONICET, Departamento de Química Teórica y Computacional, Facultad de Ciencias Químicas, Universidad Nacional de Córdoba, Córdoba 5000, Argentina*

Marcelo M. Mariscal − *Instituto de Investigaciones en Fisicoquímica de Córdoba (INFIQC) CONICET, Departamento de Química Teórica y Computacional, Facultad de Ciencias Químicas, Universidad Nacional de Córdoba, Córdoba 5000, Argentina*

José Solla-Gullón − *Institute of Electrochemistry, University of Alicante, Alicante E-03080, Spain;* orcid.org/0000-0002-9570-8110

Eugenia Zelaya − *Centro Atómico Bariloche (CAB), Comisión Nacional de Energía Atómica (CNEA)—CONICET, San Carlos de Bariloche, R8402AGP, Argentina;* orcid.org/0000-0001-7664-8936

Complete contact information is available at: https://pubs.acs.org/10.1021/acs.jpcc.0c07106

Author Contributions

The manuscript was written through contributions of all authors. All authors have given approval to the final version of the manuscript.

https://dx.doi.org/10.1021/acs.jpcc.0c07106
J. Phys. Chem. C XXXX, XXX, XXX−XXX

Funding

This work was supported in part by CONICET (PIP 0333), ANPCyT (PICT 2017-4519), Universidad Nacional de La Plata (UNLP X786) of Argentina, and Universidad Nacional de Cuyo. J.O.-A. and M.M.M. acknowledge financial support from CONICET through Grant PIP 11220150100141CO, FONCyT PICT-2015-2191, and SeCyT UNC. This work has used computational resources from CCAD, Universidad Nacional de Córdoba (http://ccad.unc.edu.ar/) and resources provided by the CYTED co-funded Thematic Network RICAP (517RT0529).

Notes

The authors declare no competing financial interest.

■ ACKNOWLEDGMENTS

J.C.A., J.O.-A., M.M.M., E.Z., and M.H.F. are research members of CONICET. N.D.A. is a CONICET fellow and a PhD student of "Facultad de Ciencias Exactas, Universidad Nacional de La Plata (UNLP)". The authors thank Dr. Valeria Palermo and Dr. Guillermo Zampieri for fruitful discussion.

■ REFERENCES

(1) Vericat, C.; Vela, M. E.; Corthey, G.; Pensa, E.; Cortés, E.; Fonticelli, M. H.; Ibañez, F.; Benitez, G. E.; Carro, P.; Salvarezza, R. C. Self-Assembled Monolayers of Thiolates on Metals: A Review Article on Sulfur-Metal Chemistry and Surface Structures. *RSC Adv.* **2014**, *4*, 27730−27754.

(2) Azcárate, J. C.; Corthey, G.; Pensa, E.; Vericat, C.; Fonticelli, M. H.; Salvarezza, R. C.; Carro, P. Understanding the Surface Chemistry of Thiolate-Protected Metallic Nanoparticles. *J. Phys. Chem. Lett.* **2013**, *4*, 3127−3138.

(3) Love, J. C.; Estroff, L. A.; Kriebel, J. K.; Nuzzo, R. G.; Whitesides, G. M. Self-Assembled Monolayers of Thiolates on Metals as a Form of Nanotechnology. *Chem. Rev.* **2005**, *105*, 1103−1170.

(4) Ben Amara, F.; Dionne, E. R.; Kassir, S.; Pellerin, C.; Badia, A. Molecular Origin of the Odd−Even Effect of Macroscopic Properties of n -Alkanethiolate Self-Assembled Monolayers: Bulk or Interface? *J. Am. Chem. Soc.* **2020**, *142*, 13051−13061.

(5) Baghbanzadeh, M.; Belding, L.; Yuan, L.; Park, J.; Al-Sayah, M. H.; Bowers, C. M.; Whitesides, G. M. Dipole-Induced Rectification Across AgTS/SAM//Ga2O3/EGaIn Junctions. *J. Am. Chem. Soc.* **2019**, *141*, 8969−8980.

(6) Singh, M.; Kaur, N.; Comini, E. The Role of Self-Assembled Monolayers in Electronic Devices. *J. Mater. Chem. C* **2020**, *8*, 3938−3955.

(7) Han, B.; Li, Y.; Ji, X.; Song, X.; Ding, S.; Li, B.; Khalid, H.; Zhang, Y.; Xu, X.; Tian, L.; et al. Systematic Modulation of Charge Transport in Molecular Devices through Facile Control of Molecule-Electrode Coupling Using a Double Self-Assembled Monolayer Nanowire Junction. *J. Am. Chem. Soc.* **2020**, *142*, 9708−9717.

(8) Karuppannan, S. K.; Neoh, E. H. L.; Vilan, A.; Nijhuis, C. A. Protective Layers Based on Carbon Paint to Yield High-Quality Large-Area Molecular Junctions with Low Contact Resistance. *J. Am. Chem. Soc.* **2020**, *142*, 3513−3524.

(9) Schwartz, J. J.; Hohman, J. N.; Morin, E. I.; Weiss, P. S. Molecular Flux Dependence of Chemical Patterning by Microcontact Printing. *ACS Appl. Mater. Interfaces* **2013**, *5*, 10310−10316.

(10) Cheung, K. M.; Stemer, D. M.; Zhao, C.; Young, T. D.; Belling, J. N.; Andrews, A. M.; Weiss, P. S. Chemical Lift-Off Lithography of Metal and Semiconductor Surfaces. *ACS Mater. Lett.* **2020**, *2*, 76−83.

(11) Ballav, N.; Shaporenko, A.; Terfort, A.; Zharnikov, M. A Flexible Approach to the Fabrication of Chemical Gradients. *Adv. Mater.* **2007**, *19*, 998−1000.

(12) Jeyachandran, Y. L.; Zharnikov, M. Comprehensive Analysis of the Effect of Electron Irradiation on Oligo(Ethylene Glycol) Terminated Self-Assembled Monolayers Applicable for Specific and Nonspecific Patterning of Proteins. *J. Phys. Chem. C* **2012**, *116*, 14950−14959.

(13) Sauter, E.; Yildirim, C.; Terfort, A.; Zharnikov, M. Adjustment of the Work Function of Pyridine and Pyrimidine Substituted Aromatic Self-Assembled Monolayers by Electron Irradiation. *J. Phys. Chem. C* **2017**, *121*, 12834−12841.

(14) Khan, M. N.; Tjong, V.; Chilkoti, A.; Zharnikov, M. Fabrication of SsDNA/Oligo(Ethylene Glycol) Monolayers and Complex Nanostructures by an Irradiation-Promoted Exchange Reaction. *Angew. Chem., Int. Ed.* **2012**, *51*, 10303−10306.

(15) Geyer, W.; Stadler, V.; Eck, W.; Zharnikov, M.; Gölzhäuser, A.; Grunze, M. Electron-Induced Crosslinking of Aromatic Self-Assembled Monolayers: Negative Resists for Nanolithography. *Appl. Phys. Lett.* **1999**, *75*, 2401−2403.

(16) Neumann, C.; Szwed, M.; Frey, M.; Tang, Z.; Kozieł, K.; Cyganik, P.; Turchanin, A. Preparation of Carbon Nanomembranes without Chemically Active Groups. *ACS Appl. Mater. Interfaces* **2019**, *11*, 31176−31181.

(17) Schmid, M.; Wan, X.; Asyuda, A.; Zharnikov, M. Modification of Self-Assembled Monolayers by Electron Irradiation: The Effect of Primary Energy (10-500 EV). *J. Phys. Chem. C* **2019**, *123*, 28301−28309.

(18) Amiaud, L.; Houplin, J.; Bourdier, M.; Humblot, V.; Azria, R.; Pradier, C. M.; Lafosse, A. Low-Energy Electron Induced Resonant Loss of Aromaticity: Consequences on Cross-Linking in Terphenylthiol SAMs. *Phys. Chem. Chem. Phys.* **2014**, *16*, 1050−1059.

(19) Shaporenko, A.; Zharnikov, M.; Feulner, P.; Menzel, D. Quantitative Analysis of Temperature Effects in Radiation Damage of Thiolate-Based Self-Assembled Monolayers. *J. Phys.: Condens. Matter* **2006**, *18*, No. S1677.

(20) Neumann, C.; Wilhelm, R.; Küllmer, M.; Turchanin, A. Low-Energy Electron Irradiation Induced Synthesis of Molecular Nanosheets: An Influence of the Electron Beam Energy. *Faraday Discuss.* **2020**, No. D00119K.

(21) Feulner, P.; Niedermayer, T.; Eberle, K.; Schneider, R.; Menzel, D.; Baumer, A.; Schmich, E.; Shaporenko, A.; Tai, Y.; Zharnikov, M. Strong Temperature Dependence of Irradiation Effects in Organic Layers. *Surf. Sci.* **2005**, *593*, 252−255.

(22) Yildirim, C.; Füser, M.; Terfort, A.; Zharnikov, M. Modification of Aromatic Self-Assembled Monolayers by Electron Irradiation: Basic Processes and Related Applications. *J. Phys. Chem. C* **2017**, *121*, 567−576.

(23) Zharnikov, M.; Geyer, W.; Gölzhäuser, A.; Frey, S.; Grunze, M. Modification of Alkanethiolate Monolayers on Au-Substrate by Low Energy Electron Irradiation: Alkyl Chains and the S/Au Interface. *Phys. Chem. Chem. Phys.* **1999**, *1*, 3163−3171.

(24) Zerulla, D.; Chassé, T. X-Ray Induced Damage of Self-Assembled Alkanethiols on Gold and Indium Phosphide. *Langmuir* **1999**, *15*, 5285−5294.

(25) Feulner, P.; Niedermayer, T.; Eberle, K.; Schneider, R.; Menzel, D.; Baumer, A.; Schmich, E.; Shaporenko, A.; Tai, Y.; Zharnikov, M. Strong Temperature Dependence of Irradiation Effects in Organic Layers. *Phys. Rev. Lett.* **2004**, *93*, 1−4.

(26) Olsen, C.; Rowntree, P. A. Bond-Selective Dissociation of Alkanethiol Based Self-Assembled Monolayers Adsorbed on Gold Substrates, Using Low-Energy Electron Beams. *J. Chem. Phys.* **1998**, *108*, 3750−3764.

(27) Huels, M. A.; Dugal, P. C.; Sanche, L. Degradation of Functionalized Alkanethiolate Monolayers by 0-18 EV Electrons. *J. Chem. Phys.* **2003**, *118*, 11168−11178.

(28) Massey, S.; Bass, A. D.; Steffenhagen, M.; Sanche, L. Oxygen Attachment on Alkanethiolate SAMs Induced by Low-Energy Electron Irradiation. *Langmuir* **2013**, *29*, 5222−5229.

(29) Seshadri, K.; Froyd, K.; Parikh, A. N.; Allara, D. L.; Lercel, M. J.; Craighead, H. G. Electron-Beam-Induced Damage in Self-Assembled Monolayers. *J. Phys. Chem. A* **1996**, *100*, 15900−15909.

(30) Kondoh, H.; Kodama, C.; Sumida, H.; Nozoye, H. Molecular Processes of Adsorption and Desorption of Alkanethiol Monolayers on Au(111). *J. Chem. Phys.* **1999**, *111*, 1175−1184.

https://dx.doi.org/10.1021/acs.jpcc.0c07106
J. Phys. Chem. C XXXX, XXX, XXX−XXX

(31) Heister, K.; Zharnikov, M.; Grunze, M.; Johansson, L. S. O.; Ulman, A. Characterization of X-Ray Induced Damage in Alkanethiolate Monolayers by High-Resolution Photoelectron Spectroscopy. *Langmuir* **2001**, *17*, 8−11.
(32) Zharnikov, M.; Frey, S.; Heister, K.; Grunze, M. Modification of Alkanethiolate Monolayers by Low Energy Electron Irradiation: Dependence on the Substrate Material and on the Length and Isotopic Composition of the Alkyl Chains. *Langmuir* **2000**, *16*, 2697−2705.
(33) Laiho, T.; Leiro, J. A.; Heinonen, M. H.; Mattila, S. S.; Lukkari, J. Photoelectron Spectroscopy Study of Irradiation Damage and Metal-Sulfur Bonds of Thiol on Silver and Copper Surfaces. *J. Electron Spectrosc. Relat. Phenom.* **2005**, *142*, 105−112.
(34) Laiho, T.; Lukkari, J.; Meretoja, M.; Laajalehto, K.; Kankare, J.; Leiro, J. A. Chemisorption of Alkyl Thiols and S-Alkyl Thiosulfates on Pt(1 1 1) and Polycrystalline Platinum Surfaces. *Surf. Sci.* **2005**, *584*, 83−89.
(35) Grumelli, D.; Cristina, L. J.; Maza, F. L.; Carro, P.; Ferro, J.; Kern, K.; Salvarezza, R. C. Thiol Adsorption on the Au(100)-Hex and Au(100)-(1 × 1) Surfaces. *J. Phys. Chem. C* **2015**, 14254.
(36) Arisnabarreta, N.; Ruano, G. D.; Lingenfelder, M.; Patrito, E. M.; Cometto, F. P. Comparative Study of the Adsorption of Thiols and Selenols on Au(111) and Au(100). *Langmuir* **2017**, *33*, 13733−13739.
(37) Cristina, L. J.; Ruano, G.; Salvarezza, R. C.; Ferron, J. Thermal Stability of Self-Assembled Monolayers of n - Hexanethiol on Au (111) - (1 × 1) and Au (001) - (1 × 1). *J. Phys. Chem. C* **2017**, *121*, 27894−27904.
(38) Salvarezza, R. C.; Carro, P. The Electrochemical Stability of Thiols on Gold Surfaces. *J. Electroanal. Chem.* **2018**, *819*, 234−239.
(39) Grumelli, D.; Maza, F. L.; Kern, K.; Salvarezza, R. C.; Carro, P. Surface Structure and Chemistry of Alkanethiols on Au(100)-(1 × 1) Substrates. *J. Phys. Chem. C* **2016**, *120*, 291−296.
(40) Hu, G.; Jin, R.; Jiang, D. E. Beyond the Staple Motif: A New Order at the Thiolate-Gold Interface. *Nanoscale* **2016**, *8*, 20103−20110.
(41) Olmos-Asar, J. A.; Rapallo, A.; Mariscal, M. M. Development of a Semiempirical Potential for Simulations of Thiol-Gold Interfaces. Application to Thiol-Protected Gold Nanoparticles. *Phys. Chem. Chem. Phys.* **2011**, *13*, 6500−6506.
(42) Azcárate, J. C.; Fonticelli, M. H.; Zelaya, E. Radiation Damage Mechanisms of Monolayer-Protected Nanoparticles via TEM Analysis. *J. Phys. Chem. C* **2017**, *121*, 26108−26116.
(43) Clavilier, J.; Armand, D.; Sun, S. G.; Petit, M. Electrochemical Adsorption Behaviour of Platinum Stepped Surfaces in Sulphuric Acid Solutions. *J. Electroanal. Chem. Interfacial Electrochem.* **1986**, *205*, 267−277.
(44) Clavilier, J. Flame-Annealing and Cleaning Technique. In *Interfacial Electrochemistry, Theory, Experiments and Applications*; Wieckowski, A., Ed.; Marcel Dekker Inc: New York, 1998; pp 231−248.
(45) Citrin, P. H.; Wertheim, G. K.; Baer, Y. Core-Level Binding Energy and Density of States from the Surface Atoms of Gold. *Phys. Rev. Lett.* **1978**, *41*, 1425−1428.
(46) Hohenberg, P.; Kohn, W. Inhomogeneous Electron Gas. *Phys. Rev.* **1964**, *136*, B864.
(47) Giannozzi, P.; Baroni, S.; Bonini, N.; Calandra, M.; Car, R.; Cavazzoni, C.; Ceresoli, D.; Chiarotti, G. L.; Cococcioni, M.; Dabo, I.; et al. QUANTUM ESPRESSO: A Modular and Open-Source Software Project for Quantum Simulations of Materials. *J. Phys.: Condens. Matter* **2009**, *21*, No. 395502.
(48) Giannozzi, P.; Andreussi, O.; Brumme, T.; Bunau, O.; Buongiorno Nardelli, M.; Calandra, M.; Car, R.; Cavazzoni, C.; Ceresoli, D.; Cococcioni, M.; et al. Advanced Capabilities for Materials Modelling with Quantum ESPRESSO. *J. Phys.: Condens. Matter* **2017**, *29*, No. 465901.
(49) Garrity, K. F.; Bennett, J. W.; Rabe, K. M.; Vanderbilt, D. Pseudopotentials for High-Throughput DFT Calculations. *Comput. Mater. Sci.* **2014**, *81*, 446−452.
(50) Perdew, J. P.; Burke, K.; Ernzerhof, M. Generalized Gradient Approximation Made Simple. *Phys. Rev. Lett.* **1996**, *77*, 3865−3868.
(51) Grimme, S. Semiempirical GGA-type density functional constructed with a long-range dispersion correction. *J. Comput. Chem.* **2006**, *27*, 1787−1799.
(52) Cleri, F.; Rosato, V. Tight-Binding Potentials for Transition Metals and Alloys. *Phys. Rev. B* **1993**, *48*, 22−33.
(53) Zharnikov, M.; Grunze, M. Modification of Thiol-Derived Self-Assembling Monolayers by Electron and x-Ray Irradiation: Scientific and Lithographic Aspects. *J. Vac. Sci. Technol., B* **2002**, *20*, 1793−1807.
(54) Duwez, A. S. Exploiting Electron Spectroscopies to Probe the Structure and Organization of Self-Assembled Monolayers: A Review. *J. Electron Spectrosc. Relat. Phenom.* **2004**, *134*, 97−138.
(55) Zhou, C.; Trionfi, A.; Hsu, J. W. P.; Walker, A. V. Electron-Beam-Induced Damage of Alkanethiolate Self-Assembled Monolayers (SAMs): Dependence on Monolayer Structure and Substrate Conductivity. *J. Phys. Chem. C* **2010**, *114*, 9362−9369.
(56) Grzeskowiak, J.; Ventrice, C. A. Low Energy Electron Interactions with 1-Decanethiol Self-Assembled Monolayers on Au(111). *J. Vac. Sci. Technol., A* **2019**, *37*, No. 051401.
(57) Zhou, C.; Jones, J. C.; Trionfi, A.; Hsu, J. W. P.; Walker, A. V. Electron Beam-Induced Damage of Alkanethiolate Self-Assembled Monolayers Adsorbed on GaAs (001): A Static Sims Investigation. *J. Phys. Chem. C* **2010**, *114*, 5400−5409.
(58) Waske, P. A.; Meyerbröker, N.; Eck, W.; Zharnikov, M. Self-Assembled Monolayers of Cyclic Aliphatic Thiols and Their Reaction toward Electron Irradiation. *J. Phys. Chem. C* **2012**, *116*, 13559−13568.
(59) Arumainayagam, C. R.; Lee, H. L.; Nelson, R. B.; Haines, D. R.; Gunawardane, R. P. Low-Energy Electron-Induced Reactions in Condensed Matter. *Surf. Sci. Rep.* **2010**, *65*, 1−44.
(60) Cometto, F. P.; Ruano, G.; Ascolani, H.; Zampieri, G. Adlayers of Alkanedithiols on Au(111): Effect of Disulfide Reducing Agent. *Langmuir* **2013**, *29*, 1400−1406.
(61) Vericat, C.; Vela, M. E.; Benitez, G. A.; Martin Gago, J. A.; Torrelles, X.; Salvarezza, R. C. Surface Characterization of Sulfur and Alkanethiol Self-Assembled Monolayers on Au(111). *J. Phys.: Condens. Matter* **2006**, *18*, No. R867.
(62) Azcárate, J. C.; Floridia Addato, M. A.; Rubert, A.; Corthey, G.; Kürten Moreno, G. S.; Benítez, G.; Zelaya, E.; Salvarezza, R. C.; Fonticelli, M. H. Surface Chemistry of Thiomalic Acid Adsorption on Planar Gold and Gold Nanoparticles. *Langmuir* **2014**, *30*, 1820−1826.
(63) Yang, Y. W.; Fan, L. J. High Resolution XPS Study of Decanethiol on Au(111): Single Sulfur-Gold Bonding Interaction. *Langmuir* **2002**, *18*, 1157−1164.
(64) Cavalleri, O.; Gonella, G.; Terreni, S.; Vignolo, M.; Pelori, P.; Floreano, L.; Morgante, A.; Canepa, M.; Rolandi, R. High Resolution XPS of the S 2p Core Level Region of the L-Cysteine/Gold Interface. *J. Phys.: Condens. Matter* **2004**, *16*, No. S2477.
(65) Azcárate, J. C.; Aagaard, N. D.; Zampieri, G.; Zelaya, E.; Fonticelli, M. H. Atomic Sulfur Formation Mechanism on 3-Mercaptopropanoic Acid Derivative Self-Assembled Monolayers: Understanding the C-S Bond Cleavage. *J. Phys. Chem. C* **2019**, *123*, 24156−24164.
(66) Arisnabarreta, N.; Ruano, G. D.; Lingenfelder, M.; Patrito, E. M.; Cometto, F. P. Comparative Study of the Adsorption of Thiols and Selenols on Au(111) and Au(100). *Langmuir* **2017**, *33*, 13733−13739.
(67) Zharnikov, M. High-Resolution X-Ray Photoelectron Spectroscopy in Studies of Self-Assembled Organic Monolayers. *J. Electron Spectrosc. Relat. Phenom.* **2010**, *178−179*, 380−393.
(68) Rodriguez, J. A.; Dvorak, J.; Jirsak, T.; Liu, G.; Hrbek, J.; Aray, Y.; González, C. Coverage Effects and the Nature of the Metal-Sulfur Bond in S/Au(111): High-Resolution Photoemission and Density-Functional Studies. *J. Am. Chem. Soc.* **2003**, *125*, 276−285.
(69) Jiang, Y.; Liang, X.; Ren, S.; Chen, C.; Fan, L.; Yang, Y.; Tang, J.; Luh, D. The Growth of Sulfur Adlayers on Au(100). *J. Chem. Phys.* **2015**, *142*, No. 064708.

https://dx.doi.org/10.1021/acs.jpcc.0c07106
J. Phys. Chem. C XXXX, XXX, XXX−XXX

(70) Brigg, D.; Beamson, G. High Resolution XPS of Organic Polymers. In *The Scienta ESCA 300 Database*; Wiley, 1992.
(71) Gelius, U.; Svensson, S.; Siegbahn, H.; Basilier, E.; Faxälv, Å.; Siegbahn, K. Vibrational and Lifetime Line Broadenings in ESCA. *Chem. Phys. Lett.* **1974**, *28*, 1−7.
(72) Heister, K.; Johansson, L. S. O.; Grunze, M.; Zharnikov, M. A Detailed Analysis of the C 1s Photoemission of N-Alkanethiolate Films on Noble Metal Substrates. *Surf. Sci.* **2003**, *529*, 36−46.
(73) Weidner, T.; Shaporenko, A.; Ballav, N.; Ulman, A.; Zharnikov, M. Modification of Alkaneselenolate Monolayers by Low-Energy Electrons. *J. Phys. Chem. C* **2008**, *112* (4), 1191−1198.
(74) Frydman, E.; Cohen, H.; Maoz, R.; Sagiv, J. Monolayer Damage in XPS Measurements as Evaluated by Independent Methods. *Langmuir* **1997**, *13*, 5089−5106.
(75) Wirde, M.; Gelius, U.; Dunbar, T.; Allara, D. L. Modification of Self-Assembled Monolayers of Alkanethiols on Gold by Ionizing Radiation. *Nucl. Instrum. Methods Phys. Res., Sect. B* **1997**, *131*, 245−251.
(76) Alloway, D. M.; Graham, A. L.; Yang, X.; Mudalige, A.; Colorado, R.; Wysocki, V. H.; Pemberton, J. E.; Lee, T. R.; Wysocki, R. J.; Armstrong, N. R. Tuning the Effective Work Function of Gold and Silver Using ω-Functionalized Alkanethiols: Varying Surface Composition through Dilution and Choice of Terminal Groups. *J. Phys. Chem. C* **2009**, *113*, 20328−20334.
(77) Buchanan, A. C.; Britt, P. F.; Thomas, K. B.; Biggs, C. A. Evidence for a Radical Relay Mechanism during Reaction of Surface-Immobilized Molecules. *J. Am. Chem. Soc.* **1996**, *118*, 2182−2189.
(78) Buchanan, A. C.; Kidder, M. K.; Britt, P. F. Molecular Orientation Effects in a Surface-Confined, Free-Radical Reaction. *J. Phys. Chem. B* **2004**, *108*, 16772−16779.
(79) Sinha, A. K.; Equbal, D. Thiol-Ene Reaction: Synthetic Aspects and Mechanistic Studies of an Anti-Markovnikov-Selective Hydrothiolation of Olefins. *Asian J. Org. Chem.* **2019**, *8*, 32−47.
(80) Dubois, L. H.; Zegarski, B. R.; Nuzzo, R. G. Molecular Ordering of Organosulfur Compounds on Au(111) and Au(100): Adsorption from Solution and in Ultrahigh Vacuum. *J. Chem. Phys.* **1993**, *98*, 678−688.
(81) Hinterwirth, H.; Kappel, S.; Waitz, T.; Prohaska, T.; Lindner, W.; Lämmerhofer, M. Quantifying Thiol Ligand Density of Self-Assembled Monolayers on Gold Nanoparticles by Inductively Coupled Plasma-Mass Spectrometry. *ACS Nano* **2013**, *7*, 1129−1136.
(82) Ballester, P.; van Leeuwer, P.; Vidal-Ferran, A. *Supramolecular Catalysis*; Elsevier Inc., 2015.
(83) Sinha, I.; Mukherjee, P. S. Chemical Transformations in Confined Space of Coordination Architectures. *Inorg. Chem.* **2018**, *57*, 4205−4221.
(84) Blobner, F.; Abufager, P. N.; Han, R.; Bauer, J.; Duncan, D. A.; Maurer, R. J.; Reuter, K.; Feulner, P.; Allegretti, F. Thiolate-Bonded Self-Assembled Monolayers on Ni(111): Bonding Strength, Structure, and Stability. *J. Phys. Chem. C* **2015**, *119*, 15455−15468.
(85) Corthey, G.; Rubert, A. A.; Benitez, G. A.; Fonticelli, M. H.; Salvarezza, R. C. Electrochemical and X-Ray Photoelectron Spectroscopy Characterization of Alkanethiols Adsorbed on Palladium Surfaces. *J. Phys. Chem. C* **2009**, *113*, 6735−6742.
(86) Rechmann, J.; Krzywiecki, M.; Erbe, A. Carbon−Sulfur Bond Cleavage During Adsorption of Octadecane Thiol to Copper in Ethanol. *Langmuir* **2019**, *35*, 6888−6897.
(87) Floridia Addato, M. A.; Rubert, A. A.; Benítez, G. A.; Fonticelli, M. H.; Carrasco, J.; Carro, P.; Salvarezza, R. C. Alkanethiol Adsorption on Platinum: Chain Length Effects on the Quality of Self-Assembled Monolayers. *J. Phys. Chem. C* **2011**, *115*, 17788−17798.

https://dx.doi.org/10.1021/acs.jpcc.0c07106
J. Phys. Chem. C XXXX, XXX, XXX−XXX